THE ASTROPHYSICAL JOURNAL, 593:1208–1216, 2003 August 20

ROLE OF MAGNETIC FLUX DISTRIBUTION IN CORONAL ENERGY STORAGE

RICHARD WOLFSON
Department of Physics, Middlebury College, Middlebury, VT 05753; wolfson@middlebury.edu
Received 2003 February 28; accepted 2003 May 5

ABSTRACT

Magnetic fields in the solar corona are most likely the dominant source of energy that powers coronal mass ejections (CMEs). Such energy must be above and beyond that of a potential (current-free) magnetic field, and thus the pre-CME coronal magnetic field should contain significant electric currents. Given the diffuse nature of the corona, the coronal magnetic field is likely to be largely force free, implying that electric currents are closely aligned with the field itself. In this work we explore such force-free fields, in the spherical geometry appropriate to the solar corona, with the aim of understanding how the magnetic flux distribution at the coronal base affects the storage of magnetic energy. We find that energy storage is enhanced when a region of strong potential field overlies a nonpotential field whose footpoints are confined to low solar latitudes. Furthermore, those flux distributions consistent with strong overlying potential fields may enable larger energy buildup, when examined in the context of limits imposed by the scalar virial theorem and the Aly-Sturrock theorem. Finally, we demonstrate the existence of force-free fields containing detached flux ropes, with energies that lie above the Aly-Sturrock limit.

Subject headings: MHD — Sun: corona — Sun: coronal mass ejections (CMEs) — Sun: magnetic fields

1. INTRODUCTION

Coronal mass ejections (CMEs) have been called "the most energetic events in the Solar System" (Klimchuk 2001). Typical CMEs expel some 10^{16} g of coronal material into interplanetary space at speeds of several hundred km s^{-1}. The energy involved, some 10^{32} ergs, is needed not only to accelerate the ejecta to such speeds, but also to lift the material against solar gravity and, most significantly, to open the coronal magnetic field so that the frozen-in plasma can escape to interplanetary space. A theorem proposed by Aly (1984, 1991) and Sturrock (1991) suggests that force-free fields alone, at least in simple geometries, are incapable of storing energy sufficient for all three of these required tasks. However, the energy associated with field-aligned currents may well supply the bulk of that energy and could, perhaps, supply all of it in more complicated magnetic geometries. In this paper, we explore energy storage in force-free fields in the spherical geometry appropriate to the solar corona. We make the simplifying assumption of axisymmetry—obviously an approximation but nevertheless one that is reflected very roughly in the large-scale structure of the solar corona. Our goal is to learn whether the distribution of magnetic flux at the coronal base plays a role in the buildup of magnetic energy in the corona. The base flux distribution is obviously a key determinant of the overall magnetic structure, and it is furthermore a quantity accessible to direct magnetograph observation.

2. CHARACTERISTIC ENERGIES OF FORCE-FREE FIELDS

Two distinct mathematical theorems place limits on the possible energies of force-free magnetic fields. The scalar virial theorem (see Priest 1984) relates surface and volume integral contributions to the energy contained in a plasma. For a force-free magnetic field in axisymmetric spherical geometry, the virial theorem takes the form

$$U = \iiint \left(B_r^2 + B_\theta^2 + B_\phi^2\right) d\tau = \iint \left(B_r^2 - B_\theta^2 - B_\phi^2\right) d\sigma \tag{1}$$

(Wolfson & Low 1992). Here $d\tau$ and $d\sigma$ are the volume and surface area elements, respectively, and $\boldsymbol{B}$ is the magnetic field, here expressed in terms of its three components in spherical polar coordinates. The left-hand integral is taken over the volume between the coronal base and some outer boundary (which may be at infinity), while the surface integral on the right is taken over the coronal base (the inner boundary) and the outer boundary. Both integrals give U, the magnetic energy, in the same arbitrary units.

In this paper we work in dimensionless units, with $r = 1$ at the coronal base. We specify the radial component of the magnetic field at the base, and in our analytic work consider that the field vanishes at infinity. In that case the surface integral on the right-hand side of equation (1) is taken over the surface of the unit sphere only. In the numerical work we take the radial field component to vanish at an outer boundary with $r \gg 1$. The reasons for this choice will be discussed shortly, but in any event if the outer boundary is sufficiently remote, numerical solutions become insensitive to the exact form of the boundary condition. More importantly in the context of equation (1), the contribution from the outer boundary to the surface integral for the magnetic energy becomes negligible for a sufficiently distant boundary. Thus, again, the virial surface integral can be taken over the inner boundary ($r = 1$) only.

Determination of a magnetostatic coronal field begins with specification of the magnetic flux distribution at the coronal base. This distribution may be stated by giving the radial field component, B_r, as a function of the polar angle θ at the coronal base ($r = 1$ in our dimensionless units). For a corona containing no electric currents, the base flux distribution, along with the boundary condition $\boldsymbol{B} = 0$ at infinity, is sufficient to determine the field everywhere. Such a field is termed a potential field, because the magnetic field, having zero curl, can be written as the gradient of a scalar potential. This potential field is strictly poloidal (no azimuthal component), and nearly all its field lines are closed and extend to finite values of r. For simple bipolar distributions the only open field lines are those originating at the poles; for more complex distributions the lines separating different flux systems are also open and extend to infinity. The energy of each such potential field is the lowest possible energy for a magnetic field with the given boundary conditions. We identify the potential field as $\boldsymbol{B}_{\rm pot}$ and its magnetic energy as $U_{\rm pot}$.

In this work we henceforth restrict ourselves to simple bipolar fields with base flux distributions symmetric about the equator, and in the present section we take the field to occupy the entire domain from the coronal base ($r = 1$) to infinity. Under these conditions, a second possible magnetic field corresponding to the same base boundary condition is potential everywhere except for a current sheet in the equatorial plane. This field becomes purely radial for $r \gg 1$, and its field lines are all open to infinity. We designate this open field as $\boldsymbol{B}_{\rm open}$ and its magnetic energy as $U_{\rm open}$.

Between the potential field and the open field lie a range of force-free magnetic fields whose field lines' magnetic footpoints are displaced in azimuthal angle, giving rise to a toroidal field component B_ϕ. These fields have the same distribution of magnetic flux at the coronal base—that is, the same B_r versus θ—as do $\boldsymbol{B}_{\rm pot}$ and $\boldsymbol{B}_{\rm open}$, but these fields are not fully determined by the base flux distribution. Rather, one must also specify either the toroidal component or the footpoint separation—the so-called magnetic shear. The Aly-Sturrock theorem (Aly 1984, 1991; Sturrock 1991) states that the energies of these sheared fields must lie below $U_{\rm open}$, at least as long as the field contains no disconnected magnetic flux. A look at the virial surface integral in equation (1) shows that, at least on average, B_θ must decrease as B_ϕ increases in order for the sheared-field energy to rise above $U_{\rm pot}$. Therefore the poloidal field must become more nearly radial at the base, and so the field lines should bulge outward as the magnetic shear increases. Physically, the sheared field tends to look more like the open field as shear increases, so it makes sense that the sheared-field energy approaches but does not exceed $U_{\rm open}$. This observation is, however, just a plausibility argument and is certainly not an ironclad assertion of the Aly-Sturrock theorem. We designate any of these infinitely many sheared force-free fields as $\boldsymbol{B}_s$ and the corresponding energy by U_s.

Finally, the surface integral for the magnetic energy on the right-hand side of equation (1) shows that there is an absolute maximum possible energy for any force-free field with a given flux distribution at the coronal base. This energy, designated $U_{\rm max}$, is obtained by setting $B_\theta = B_\phi = 0$ and thus integrating only B_r^2. The field with this particular energy is strictly radial everywhere, and is generally neither potential nor force-free. It is of interest less as a realizable magnetic field than as evidence for an absolute upper bound on the energies of force-free fields.

To summarize, we have identified three distinct magnetic energies associated with fields that share a common flux distribution at the coronal base: $U_{\rm pot}$, the energy of the everywhere current-free field; $U_{\rm open}$, the energy of the field whose lines are all open to infinity and that is current-free everywhere except on a current sheet in the equatorial plane; and $U_{\rm max}$, the maximum possible energy for any force-free field. These fields obey the inequality

$$U_{\rm pot} < U_{\rm open} \leq U_{\rm max} \ . \tag{2}$$

(The reason for the possible equality in the relation between $U_{\rm open}$ and $U_{\rm max}$ will become obvious shortly.) In addition to these three discrete fields, we have an infinite set of force-free fields whose energies must lie between $U_{\rm pot}$ and $U_{\rm max}$. For force-free fields whose field lines are all anchored at the coronal base, the Aly-Sturrock theorem further restricts the maximum energy to $U_{\rm open}$.

3. BASE FLUX DISTRIBUTIONS AND ENERGIES

It proves convenient to express the poloidal components of the magnetic field in terms of a flux function $\psi(r, \theta)$, which in our axisymmetric spherical geometry is $A_\phi r \sin\theta$, with $\boldsymbol{A}$ the magnetic vector potential. In terms of ψ, the entire magnetic field becomes

$$\boldsymbol{B} = \frac{1}{r^2 \sin\theta}\frac{\partial\psi}{\partial\theta}\hat{\boldsymbol{r}} - \frac{1}{r\sin\theta}\frac{\partial\psi}{\partial r}\hat{\boldsymbol{\theta}} + B_\phi\hat{\boldsymbol{\phi}} \ , \tag{3}$$

where the toroidal component B_ϕ is as yet unspecified. For the potential fields discussed in this section, $B_\phi = 0$, and the contours of ψ are the magnetic field lines. Later, with force-free fields where $B_\phi \neq 0$, the contours of ψ will represent the projections of the field lines on (r, θ) planes.

The boundary condition at the coronal base can be specified by giving $\psi(1, \theta)$; the actual radial field component at the base then follows from equation (3).

In this work we consider base boundary conditions described by

$$\psi(\mu) = \psi_0(1 - |\mu|^\alpha) \ , \tag{4}$$

where $\mu = \cos\theta$ and ψ_0 is a parameter that sets the overall scale of the magnetic field. The important parameter is α, which determines the distribution of magnetic flux at the coronal base. The case $\alpha = 2$ describes the boundary conditions appropriate to a dipole field; here, equation (3) shows that $B_r(r = 1) \propto \mu$. Since $\mu = \cos\theta$, this is the well-known result for the angular dependence of the radial component of a dipole field. More generally, equations (3) and (4) give

$$B_r(r = 1) = \pm\psi_0\alpha|\mu|^{\alpha-1} \ , \tag{5}$$

where the positive and negative signs apply to the northern and southern hemispheres, respectively.

The choice $\alpha = 1$ is the boundary condition appropriate to the "split monopole," widely used in solar physics to represent a strictly radial field that reverses sign across the equatorial plane. In this case, as equation (5) shows, the field at the coronal base is independent of polar angle (i.e., of μ), except for the abrupt reversal at the equator. For the split monopole ($\alpha = 1$), magnetic flux is thus distributed evenly in colatitude. For the dipole ($\alpha = 2$), $B_r \propto \mu = \cos\theta$, and flux is concentrated more toward the solar poles. Indeed, this is true for any $\alpha > 1$, and the poleward shift of flux continues as α surpasses the dipole value 2 and increases further. Our choice of the form given in equation (5) is motivated in part by the desire for a simple expression in which a variation of a single parameter changes the flux distribution in a physically meaningful way, and in part because of previous work in which the mathematics of a separable solution changes the boundary condition in a way that corresponds roughly to a change from $\alpha = 2$ to $\alpha = 1$ in equation (5) (Lynden-Bell & Boily 1994; Wolfson 1995).

In § 2, we identified three discrete energies associated with magnetic fields sharing a common base flux distribution. Here, we calculate the energies of those fields. For the energy $U_{\max}$, it suffices to integrate the square of the base radial field given by equation (5); for the energies of the purely potential field and of the open field, it is necessary first to know also the transverse field component at the base. Although it would be possible to solve for these fields using potential theory (recall that even the open field is potential everywhere except on an equatorial current sheet), it is more convenient to solve in terms of the flux function ψ introduced earlier, as this approach will be necessary when solving for nonpotential fields.

For a potential field in axisymmetric spherical geometry, the flux function ψ is governed by the equation

$$\frac{\partial^2\psi}{\partial r^2} + \frac{1-\mu^2}{r^2}\frac{\partial^2\psi}{\partial\mu^2} = 0 \qquad (6)$$

(Wolfson & Low 1992). This linear equation is separable, and we have shown that it admits solutions of the general form

$$\psi = \sum_{l=0}^{\infty}\left(a_l r^{-l} + b_l r^{l+1}\right)\left[\frac{P_{l-1}(\mu) - P_{l+1}(\mu)}{2l+1}\right]. \qquad (7)$$

Here the a_l and b_l are coefficients to be determined, P_l is the lth Legendre polynomial, and $r, \mu = \cos\theta$ are the spherical polar coordinates (Wolfson 1985).

For a closed, bipolar field in the domain from $r = 1$ to $r = \infty$, the boundary condition at infinity is simply $\psi = 0$, so only the a_l are nonzero. In this case the sum in equation (7) is taken over odd l only, resulting in even Legendre polynomials in the expression for ψ. It then follows from equation (3) that B_r is an odd function of μ, showing that its sign reverses across the equator, while B_θ is even—characteristics of any bipolar field whose field lines are symmetric about the equatorial plane. In the Appendix we show explicitly how the coefficients a_l are calculated from the boundary condition given by equation (4).

For the open field, the presence of the equatorial current sheet requires different series solutions in the two hemispheres (although the two are related by a simple sign change). In this case we require that the transverse field vanish in the equatorial plane ($\mu = 0$) and also at infinity. These conditions make equation (7) a series in odd Legendre polynomials, plus a constant term (formally involving the even polynomial $P_0 = 1$). Again, the Appendix gives the details for determining the coefficients a_l.

Given the appropriate Legendre series solutions, we can evaluate the virial surface integral in equation (1) to determine the energies of the closed, open, and maximum-energy fields for different values of the parameter α. In practice, we calculate the coefficients out to a maximum l value of 21, differentiate the series according to equation (3), and then evaluate the virial surface integral for the energy. All these calculations are done analytically using MATHEMATICA. A graphical comparison shows that the truncated series solutions reproduce the base distributions of equation (4) to better than 1 part in 10^{16}.

Figure 1 shows the results of these energy calculations. For comparison purposes, we have normalized the energies

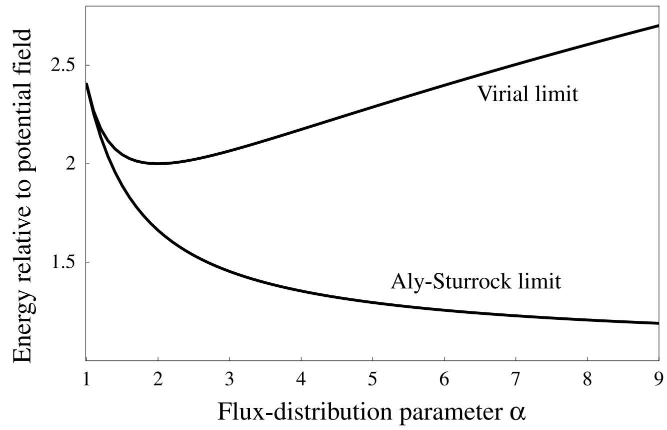

FIG. 1.—Energy of the Aly-Sturrock open field and the maximum possible energy for any force-free field, as set by the virial theorem, as functions of the parameter α. Larger α values correspond to a greater concentration of flux at higher latitudes. Both energies are in units of the potential-field energy for each value of α.

so that the potential-field energies for different values of α are all taken as 1. This choice to normalize energies means that the base magnetic field strengths at a fixed point—say, the pole—are different for different α. An alternative would have been to fix the base field at the pole, and then express all energies in terms of the energy of the potential dipole. However, our energy-normalization approach seems more appropriate in the context of comparisons among the three characteristic energies $U_{\rm pot}$, $U_{\rm open}$, and $U_{\max}$.

Given this normalization, the two curves in Figure 1 give the open-field and maximum possible energies for each α in terms of the potential-field energy for that same α. Note that for $\alpha = 1$ (the split monopole) the two energies are the same. In this case the open field, potential everywhere except on the equatorial current sheet, is strictly radial and is thus the same as the maximum-energy field. This equality of $U_{\rm open}$ and $U_{\max}$ at $\alpha = 1$ shows that, with this base flux distribution, there is absolutely no possibility of force-free fields whose energy lies above the Aly-Sturrock open-field limit. This equality is also the reason for the greater-than-or-equal sign in inequality (2). For $\alpha > 1$, the $U_{\rm open}$ and $U_{\max}$ curves diverge, creating an energy gap that could, in principle, be occupied by force-free fields not subject to the Aly-Sturrock theorem (e.g., fields containing disconnected flux). As α increases—physically, as flux concentrates toward the poles—the gap grows. This occurs in part because of the growth in $U_{\max}$, but more significantly because the ratio of $U_{\rm open}$ to $U_{\rm pot}$ shrinks. Physically, this may make it energetically easier to bring a magnetic field with larger α—more flux concentrated at higher latitudes—to energies approaching the open-field energy $U_{\rm open}$.

4. FORCE-FREE FIELDS

Here we develop the basic equations for sheared, force-free magnetic fields with different flux distributions as specified by the parameter α. In our axisymmetric geometry, the combination of Ampère's law,

$$\boldsymbol{J} = \frac{c}{4\pi}\nabla\times\boldsymbol{B}, \qquad (8)$$

and the force-free condition $\boldsymbol{J}\times\boldsymbol{B} = 0$ leads to a Grad-

Shafranov type of equation for the flux function ψ,

$$\frac{\partial^2\psi}{\partial r^2}+\frac{1-\mu^2}{r^2}\frac{\partial^2\psi}{\partial\mu^2}=-f\frac{df}{d\psi} \tag{9}$$

(Wolfson 1995).

Here $f(\psi)$ is an arbitrary function of the flux function ψ, related to the azimuthal field component by

$$B_\phi=\frac{f(\psi)}{r\sin\theta}\ . \tag{10}$$

The footpoint shear associated with a given $f(\psi)$ can be calculated by integration over the field lines, once the solution ψ has been found.

The function f (or, more accurately, the quantity $-fdf/d\psi$) is called the generating function, and its use has been criticized as being a less physical approach to the problem than the direct specification of the footpoint shear—as is possible when the field is expressed in terms of Clebsch variables (Antiochos, Devore, & Klimchuk 1999). One problem with the generating-function approach is that it can lead to solution sequences that exhibit unphysical or pathological behavior as the amplitude of the generating function is increased. Absent such behavior, though, solutions obtained by the generating-function method represent perfectly valid force-free fields.

The main criticism leveled against the generating-function approach focuses on a Cartesian geometry solution by Low (1977), in which a critical value of the generating-function amplitude results in a " tear " in the magnetic field, such that magnetic footpoints originally infinitesimally close end up a finite distance apart (Klimchuk & Sturrock 1989). Here we avoid that possibility by choosing a generating function whose value and derivative both vanish at the equator—meaning that the magnetic shear is zero on the infinitesimally separated footpoints of the lowest magnetic field lines that just cross the equator. Specifically, we take the function $f(\psi)$ to be given by

$$f(\psi)=\gamma\sin\left[\pi\left(\frac{\psi-\psi^*}{\psi_0-\psi^*}\right)^2\right],\quad \psi^*<\psi<\psi_0$$

and

$$f(\psi)=0,\quad \psi>\psi_0 \text{ or } \psi<\psi^*\ . \tag{11}$$

Here γ is a parameter loosely related to the amount of shear applied to the magnetic footpoints. The quantity ψ_0 is the value of the flux function at $r=1$, $\theta=\pi/2$, and is chosen so that the energy given by equation (1) has the value 1 in the potential-field case ($\gamma=0$). Finally, the constant ψ^* is set, through equation (4), to confine the shear to a region equatorward of a fixed latitude, here taken to be 45°. The effect of this confinement is to produce a sheared force-free field that lies beneath a potential field, with the strength of the overlying potential field growing as the parameter α increases.

For the dipole field ($\alpha=2$), at low shear, integration over the field lines shows that the shear is given by

$$\Delta\phi=\frac{2\cos\theta}{\gamma\psi_0\sin^4\theta}f(\psi)\ . \tag{12}$$

This profile is shown in Figure 2. As the shear increases the profile changes somewhat, but remains qualitatively similar (see Wolfson & Low 1992 for a discussion of this " pseudo–shear-specified " approach). For other base flux distributions ($\alpha\neq2$), the shear profile is similar but not identical.

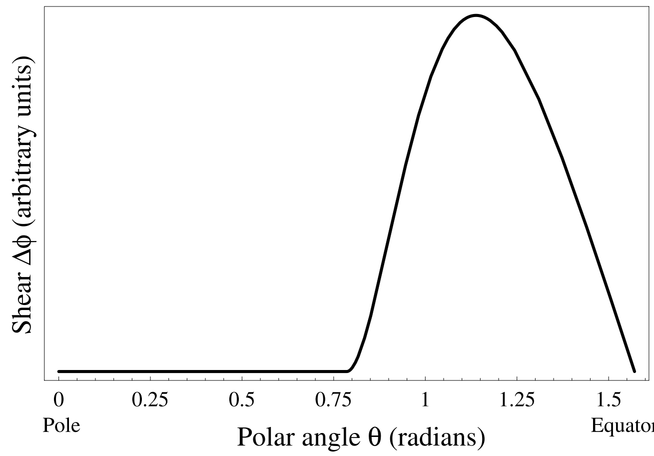

FIG. 2.—Typical shear profile, giving the angular separation in azimuthal angle ϕ between northern and southern hemisphere magnetic footpoints, as a function of the polar angle at the NH footpoint. Profile shown is for the dipole flux distribution ($\alpha=2$), at low values of γ. The profile amplitude scales with γ, while the profile shape changes only slightly as γ increases.

5. NUMERICAL ISSUES

The computation of force-free magnetic fields is a more formidable numerical problem than it might at first seem. Our equation (9) is, mathematically, a nonlinear elliptic partial differential equation in two independent variables. Analytic and numerical methods for linear elliptic PDEs are widely available, and iterative approaches can be applied in nonlinear cases. In previous work on nonlinear force-free fields, we have used finite-difference methods, employing available linear solvers embedded in iterative schemes (see Wolfson & Low 1992). Those methods proved reliable except at extreme shears, where convergence could become problematic. In the present study, we have developed a numerical code based on the finite-element method. In this method, widely used in engineering but less familiar to astrophysicists, the domain of the problem is broken into small geometrical elements, in our case triangles. The solution in each triangle is represented by a function of two variables, in this case a simple linear function. The parameters in each finite element's solution function are then determined by solving a variational problem that optimizes the fit of the global solution to the partial differential equation. One advantage of the finite-element method is that the solution and its derivatives are defined at all points in the domain, not just at the nodes as is the case with finite-difference discretization. A second advantage is the ease of producing nonuniform meshes, and adaptively refining the mesh based on a posteriori error estimates. Finally, the finite-element method lends itself to irregular domains—those whose boundaries do not lie on coordinate surfaces.

At the heart of our force-free approach is the finite-element code PLTMG (for Piecewise Linear Triangle MultiGrid), a robust and versatile two-dimensional nonlinear elliptic solver (Bank 1998). The code is now in its eighth version and is freely available. PLTMG incorporates a

Newton iteration scheme that makes the code explicitly applicable to nonlinear problems. It also has built-in evaluation of user-specified integrals over the solution domain and/or boundary, making it easy to track values of the energies given in equation (1). Finally, the code includes a continuation procedure for following solution sequences generated by varying one parameter in the PDE. However, we have not employed this procedure in the present work—although we have effectively done the same thing through an adaptive stepsize procedure in the parameter γ that appears in our function $f(\psi)$.

PLTMG also has powerful visualization capabilities, embodied in a set of graphical output routines. These routines assume a Cartesian-like geometry, and for that reason we have transformed equation (9) to cylindrical coordinates ρ, z, which, although still properly describing our axisymmetric spherical geometry, allow Cartesian-like graphics in the ρ-z plane. Transformation of equation (9) to cylindrical coordinates is straightforward, and results in the equation we actually solve with PLTMG:

$$\frac{\partial^2\psi}{\partial\rho^2} - \frac{\partial}{\partial\rho}\left(\frac{\psi}{\rho}\right) + \frac{\partial^2\psi}{\partial z^2} = \frac{\psi}{\rho^2} - f\frac{df}{d\psi}\,. \tag{13}$$

Because PLTMG accepts irregular boundaries—and is especially welcoming of circular arc boundaries—we can easily continue to define the problem in a domain from $r = 1$ to some spherical outer boundary at $r = r_{\rm max}$. In what follows we generally take $r_{\rm max} = 20$, although we have shown explicitly that increasing $r_{\rm max}$ has negligible effect on the computed energies. Although one could solve this problem on the half-domain from pole to equator, with a boundary condition $B_r = 0$ in the equatorial plane, we choose instead the computationally less efficient approach of computing over the entire range $0 \leq \theta \leq \pi$. That way the equatorial plane is not a boundary, and thus we allow for the possibility that current sheets might form in the equatorial plane. However, that possibility is not realized in the calculations reported here.

PLTMG generates its own mesh from a simple specification of the solution domain. Our computational mesh calls for 10,000–40,000 vertices, and the resulting number of finite element triangles is approximately twice this number. The higher resolutions are required for consistent convergence at the larger values of the flux-distribution parameter α. We solve first the potential-field problem, first on a coarser mesh and then, using PLTMG's adaptive refinement, approaching the final mesh of some 10^4 vertices in a way that puts more and smaller elements where the solution gradients are greatest (see Fig. 3 for a sample finite-element mesh). We then verify that the flux function, magnetic field, and both energy integrals are essentially equal to those of the analytic Legendre series solutions introduced earlier. On occasion it is necessary to refine the mesh further, either at this point or later in the calculational sequence, in order to keep the a posteriori error estimates below a specified tolerance.

For a given value of the flux-distribution parameter α, we then generate a sequence of solutions corresponding to increasing values of the parameter γ that specifies the deviation from a potential field. We calculate both volume and surface integrals for the magnetic energy associated with each solution, and compare the two. The sequence is assumed to terminate under any of the following conditions:

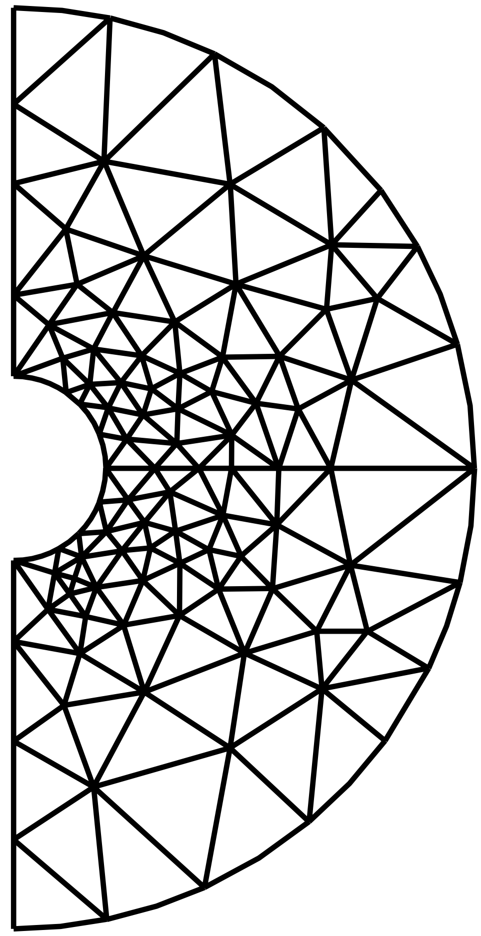

FIG. 3.—Sample finite-element mesh, with 300 vertices, refined to put more elements where the potential dipole solution has the largest gradients. Actual meshes used in numerical calculations have between 10,000 and 40,000 vertices, and are refined adaptively as needed.

(1) the two energy integrals disagree by more than 6%; (2) the nonlinear solver fails to converge; or (3) the solution exhibits features clearly inconsistent with a force-free field or even, on occasion, with Ampère's law itself. (The latter case occurs if the code produces magnetic islands containing values of the flux function greater than ψ_0, for which eq. [11] shows that the field must be potential.)

This list of difficulties, all of which occur at large values of magnetic shear (high values of γ), might sound like serious flaws in a code that is, after all, supposed to produce force-free solutions. On comparison with other methods, however, ours seems remarkably stable up to these most extreme magnetic shears. One issue with this and any other force-free code is to test whether the resulting solution is, in fact, force free. Perhaps the most straightforward approach is to calculate the angle between the current density $\boldsymbol{J}$ and magnetic field $\boldsymbol{B}$. However, this presents a problem for any method based on a vector potential, flux function, or Clebsch variables, in all of which the magnetic field must be computed as a numerical first derivative and the current density as a second derivative. Because numerical differentiation is an inherently error-amplifying procedure, the calculation of the angle between $\boldsymbol{J}$ and $\boldsymbol{B}$ is not particularly accurate. A second approach is to test the validity of the virial theorem described in equation (1), which of course must be satisfied exactly by a strictly force-free field. This amounts to comparing the two different integrals for the magnetic energy, which should be equal for a force-free field. This approach has the advantage of integrating over numerically computed first derivatives, greatly reducing the error—especially in the case of the volume integral for the magnetic energy. The surface integral is more problematic, because the field components must be computed from derivatives taken at the boundary, and these particular derivatives are generally only first-order accurate as opposed to the typically second-order accuracy that obtains in the interior of the solution domain. For that reason the two integrals in equation (1) generally differ by a few percent, even at low values of γ. That is the reason for our somewhat arbitrary 6% criterion for accepting a solution as force free.

Another popular approach to force-free fields is the magnetofrictional method (Yang, Sturrock, & Antiochos 1986; Antiochos et al. 1999), in which a pseudo–time-dependent problem is solved essentially by moving the magnetic field in response to a computed Lorentz force until that force becomes negligible. This method has the distinct advantage of specifying directly the footpoint shear (through one of the two Clebsch variables used to represent the magnetic field), thus avoiding the criticisms that apply to the generating-function method. We have obtained and studied a particular magnetofrictional code written for force-free problems in spherical geometry (Antiochos et al. 1999). This code checks the solution by computing a current-weighted average of the cosine of the angle between $\boldsymbol{J}$ and $\boldsymbol{B}$, and the results are impressive: after tens of thousands of iterations, this average cosine is generally within 10^{-4} or better of the exact force-free value, namely, 1. However, after adapting the magnetofrictional code to test also conformance with the virial theorem, we find that the volume and surface integrals for the magnetic energy often differ dramatically—sometimes by factors of 20 or more—and that the surface integral is frequently negative. These discrepancies occur despite average-cosine results that suggest a nearly perfectly force-free solution. Even with the finest mesh, the two integrals differ by more than 10% well before reaching anything approaching extreme values of shear. And at more extreme shears, the magnetofrictional method exhibits its own difficulties with convergence. Furthermore, at lower resolutions, this magnetofrictional code can in some cases report a force-free solution based on the cosine criterion, while the volume energy integral gives values above even the maximum allowed by the virial theorem.

Clearly, it is no simple matter to verify that a numerical solution is indeed force free. Again, our criterion in the present study is that the solution satisfy the virial theorem for force-free fields. As described above, the solution is obtained by solving a generating-function-containing nonlinear elliptic PDE using the finite-element code PLTMG.

6. RESULTS

For each value of the flux distribution parameter α, our method produces a sequence of solutions for increasing values of the parameter γ. At $\gamma = 0$ we get excellent agreement with our analytic Legendre series solutions, and the two integrals for magnetic energy are in close agreement. As γ increases, the magnetic field bulges outward somewhat, and both energy integrals increase together. Eventually the energies begin to rise more rapidly, as measured by the derivative $dU/d\gamma$. At this point we employ an adaptive stepsize in γ to limit the increase in energy with each step. Eventually $dU/d\gamma$ reaches a very large value at which we consider the energy to be the maximum possible in a closed arcade with this particular value of α and the form we have adopted for the function f. Increasing γ still further results in one of several possibilities:

1. A sequence of similar solutions with energies and field configuration changing only slightly and in a stochastic way. We suspect these are essentially the same solution, reached through slightly different nonlinear Newton iteration paths.
2. Convergence failure in the numerical method.
3. A rapid divergence of the two energy integrals, usually with the volume integral increasing much more than the surface integral, and indicating that the solution is no longer truly force free.
4. The appearance of chaotic field structure on small scales, which we take to indicate a failure of the numerical method.
5. The development of X-O neutral point pairs, and associated detached magnetic flux ropes.

Of these possible outcomes, probably only 5, with detached flux ropes, is physically meaningful.

Figure 4 shows the energies calculated for numerical solutions with the flux-distribution parameter α ranging from 1 to 9, stepping by $\Delta\alpha = 0.1$ In contrast to Figure 1, we have normalized the energies in Figure 4 to the energy of the analytic open-field solution—the maximum allowed by the Aly-Sturrock theorem for force-free fields without detached flux. The irregularities in the numerical-solution energy curves in Figure 4 reflect the difficulties in obtaining consistent convergence near what is a critical point in the solution sequence. Nevertheless, the overall trend is quite obvious. Energies of the maximally sheared arcade solutions evidently track the potential-field energies, but are of course

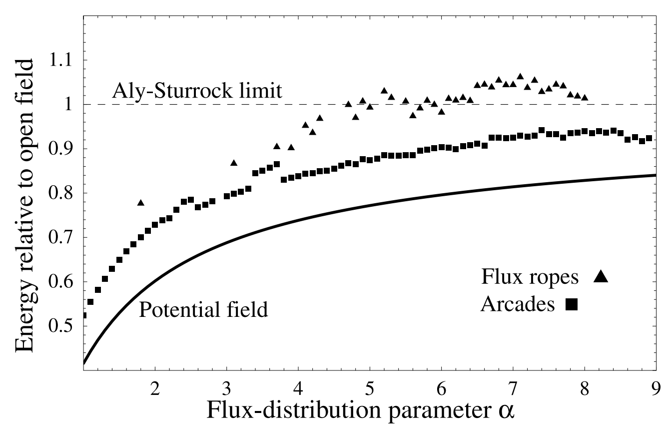

FIG. 4.—Energies of numerical solutions, normalized to 1 at the Aly-Sturrock open-field limit. Squares mark maximum-energy sheared arcades and triangles are flux rope solutions. Convergence of flux rope solutions was unreliable beyond $\alpha = 8$ and, with the one exception shown, below about $\alpha = 3$. The considerable scatter suggests that energies of the numerical solutions are not accurately determined, and that flux rope energies above the Aly-Sturrock limit cannot be taken as definitive evidence of force-free fields with energies in excess of that limit—even though such energies are allowed for detached flux ropes. Also shown are the potential-field energies, again normalized to the open-field limit.

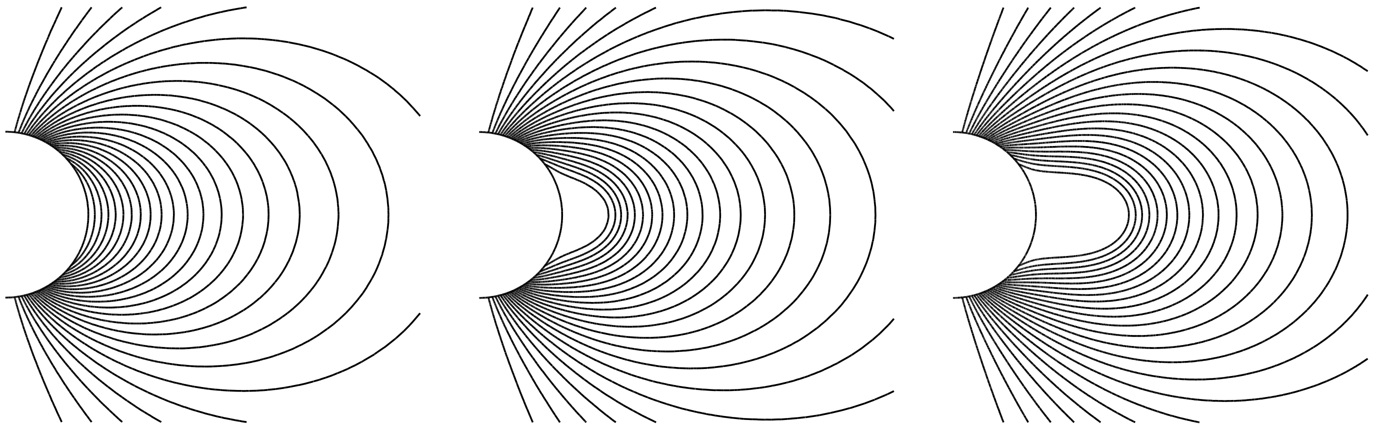

FIG. 5.—Projections of magnetic field lines in the poloidal plane, for the potential field (*left*), the maximally sheared field (*center*), and the flux rope solution (*right*), all for $\alpha = 6.6$. Circular arc at left is the solar surface, and the plots show a limited portion of solutions that were computed out to 20 $R_\odot$. The sheared region involves those field lines whose footpoints lie within 45° of the solar equator. With the linear contouring routine used here, the rightmost frame does not show the flux rope itself. The rope is shown in detail in Fig. 6.

higher. At the higher α values, the maximally sheared arcade energies are some 90% of the open-field Aly-Sturrock limit (the value 1 in Fig. 4). This result confirms our earlier suggestion, based on the analytic calculations alone, that it may be easier to build up substantial magnetic energy in a sheared force-free field when a strong potential field overlies the sheared field.

The curve for flux rope solutions in Figure 4 is particularly interesting, since it shows some solutions with energies in excess of the Aly-Sturrock limit. This situation is permitted because these fields include detached magnetic flux; however, we know of no clear demonstration in the literature of the existence of such force-free solutions with detached flux that exceed the Aly-Sturrock energy. Because of the uncertainties in the numerical energy calculations, and the fact that the flux rope energies are only a few percent over the Aly-Sturrock limit, ours should not be taken as such a demonstration either. Nevertheless, it is intriguing that our method produces flux rope solutions with substantially more energy than those of fully attached magnetic arcades, and that the energies of those flux rope solutions are in the vicinity of the Aly-Sturrock limit.

Figure 5 shows field line projections on the poloidal plane, plotted for the potential field, maximally sheared arcade, and flux rope solutions. The evolving field exhibits the gradual bulging expected from the buildup of energy associated with the increasing toroidal field component. This bulging is most significant in the lower corona, but has less effect on the overlying potential field whose footpoints lie beyond 45° solar latitude. For the solutions shown, $\alpha = 6.6$, meaning there is very little flux emerging near the solar equator. The linear contouring routine therefore does not show the innermost field lines, and in particular does not show the flux rope that, in the rightmost frame, underlies the innermost field line shown.

A more detailed look at the flux rope solutions proves most interesting. The form we have assumed for the function $f(\psi)$, as given by equation (11), precludes the emergence of an X-O neutral point pair through the coronal base. This is because such a pair would entail values of the flux function ψ in excess of ψ_0, and our choice of f ensures that f, and therefore B_ϕ, must be zero for such values $\psi > \psi_0$. Field lines with $\psi > \psi_0$ therefore could not satisfy Ampère's law because they would have to form closed loops and yet could not encircle any electric current. However, X-O pairs can form with ψ in the range where f is nonzero. Physically, such a change in solution topology could not occur in ideal MHD, but that is not an issue here because we are not concerned with physically realistic temporal evolution of the coronal magnetic field, but only with demonstrating the existence of solutions with particular magnetic energies.

Figure 6 shows that the flux rope solution is interestingly complicated, containing not one but two distinct ropes. There are correspondingly two each of X and O neutral points. An examination of Figure 6 in the context of

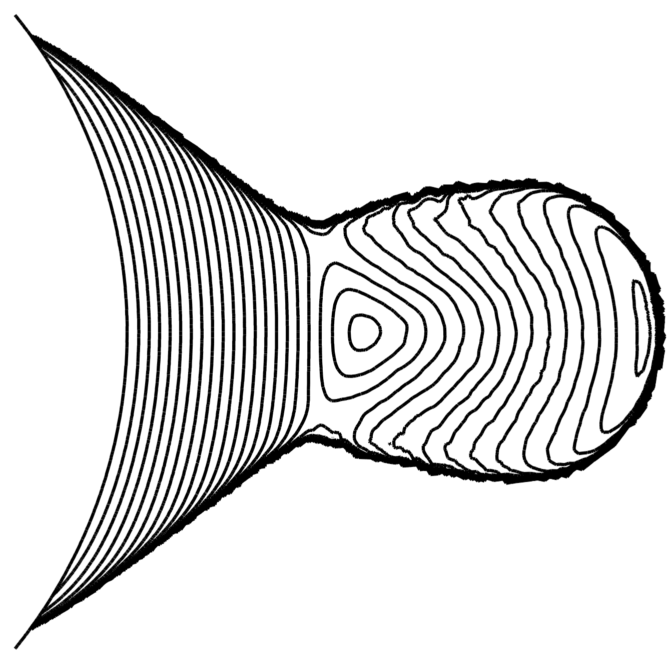

FIG. 6.—Details of the flux rope solution shown in the rightmost frame of Fig. 5. There are actually two flux ropes, and two each of X- and O-type neutral points. The apparent bunching of field lines at the edges of the figure is an artifact resulting from a highly nonlinear contouring scheme needed to show the flux rope field lines. Arc at left represents the solar limb.

Ampère's law shows that the toroidal currents in the two ropes must be in opposite directions. Although our model is too idealized to be an accurate representation of the corona, the appearance of this flux rope pair is intriguing. The outer rope, with its squashed, "kidney" shape, looks not unlike some sketches depicting magnetic clouds observed in interplanetary space. Such clouds are believed to be the interplanetary manifestations of CMEs. And although mass plays no role in our model except to carry electric current, and therefore there is nothing like a prominence in the model, it is interesting to speculate that the lower flux rope might correspond to the cavity that is often inhabited by a prominence.

Comparison of the poloidal and toroidal field components in the equatorial plane shows that the field is almost entirely toroidal inside the flux ropes. Therefore, the ropes exhibit only a very weak twist. The center of the inner flux rope, which corresponds to a broad, shallow local minimum in the flux function ψ, occurs at very nearly the value at which the function $f(\psi)$ has its maximum. The outer rope corresponds to a sharply peaked local maximum in ψ, although with a value only slightly different from that of the inner rope. Both these ψ values lie somewhat closer to the equatorial base value ψ_0 than to ψ^*.

We have been frustrated in attempting to explore in detail the formation of the double-flux rope solution. Practically, our numerical procedure seems incapable of resolving the "instant" at which the flux ropes form, but rather jumps abruptly from a closed arcade solution to one containing flux ropes. Or it may be that the solution sequence reaches a catastrophe point (see Forbes & Isenberg 1991) where $dU/d\gamma$ becomes infinite, and then jumps abruptly to a new solution with the flux rope topology.

7. CONCLUSION

We have computed force-free magnetic fields appropriate to the spherical geometry of the solar corona, for a wide range of magnetic flux distributions at the base of the model corona. Our results show that it may be easier for shearing of the magnetic footpoints to build up energy approaching the Aly-Sturrock open-field limit when a strong potential field overlies the sheared field. Furthermore, we find that under that same condition, our solutions develop flux ropes with energies that seem to be slightly in excess of the Aly-Sturrock limit—although numerical noise prevents us from drawing that conclusion with certainty. To the extent that our results reflect physical processes in the real corona, they suggest that substantial energy storage, and thus the potential for coronal mass ejections, may be greatest in regions of the corona where a strong potential magnetic field overlies a region where footpoint shear is occurring.

This work was supported by NASA grant NAG 5-9733 to Middlebury College. We thank Spiro Antiochos of the Naval Research Laboratory for supplying the magnetofrictional code discussed in this paper, and Randolph Bank of University of California, San Diego, for his many consultations on the finite element code PLTMG.

APPENDIX A

LEGENDRE SERIES SOLUTIONS

We have previously shown (Wolfson 1985) that equation (6) has the general solution given in equation (7):

$$\psi = \sum_{l=0}^{\infty}\left(a_l r^{-l} + b_l r^{l+1}\right)\left[\frac{P_{l-1}(\mu) - P_{l+1}(\mu)}{2l+1}\right] . \tag{A1}$$

For closed fields, with the boundary condition $\psi = 0$ at $r = \infty$, it suffices to set all the b_l to zero. Then to meet the base boundary condition of equation (4), we multiply equation (A1) by $\psi_0(1 - |\mu|^{\alpha})P_m(\mu)$ and integrate over the polar angle (i.e., from $\mu = -1$ to 1). Using the orthogonality properties of the Legendre polynomials, the result becomes

$$2\psi_0 \int_0^1 (1 - \mu^{\alpha})P_m(\mu)\, d\mu = \frac{2}{2m+1}\left(\frac{a_{m+1}}{2m+3} - \frac{a_{m-1}}{2m-1}\right) , \tag{A2}$$

where symmetry allows us to take the integral from 0 to 1 and double the result, also dropping the absolute value signs. Designate the integral here by I_{mc} (c for closed field):

$$I_{mc} = \int_0^1 (1 - \mu^{\alpha})P_m(\mu)\, d\mu ,$$

so

$$2\psi_0 I_{mc} = \frac{2}{2m+1}\left(\frac{a_{m+1}}{2m+3} - \frac{a_{m-1}}{2m-1}\right) .$$

This equation can be written in the form of a recursion relation:

$$a_{m+1} = (2m+3)\left[(2m+1)\psi_0 I_{mc} + \frac{a_{m-1}}{2m-1}\right] . \tag{A3}$$

We start with the case $m = 0$, which gives

$$a_1 = \tfrac{3}{2} I_{0c} .$$

The other nonzero coefficients, all odd and thus resulting through equation (A1) in even Legendre polynomials reflecting the equatorial symmetry, are then obtained through the recursion relation (A3).

The open-field case is handled in a similar way, except that now all field lines are required to extend to infinity. So we replace the closed-field boundary condition at infinity, $\psi = 0$, with $B_\theta = 0$. Equivalently, $d\psi/dr = 0$ at infinity. Differentiation of equation (A1) gives

$$\frac{\partial \psi}{\partial r} = \sum \left[-la_l r^{-(l+1)} + (l+1) b_l r^l \right] \left[\frac{P_{l-1}(\mu) - P_{l+1}(\mu)}{2l+1} \right] , \tag{A4}$$

showing that all the b_l must vanish to meet the condition $d\psi/dr = 0$ at infinity. In order that ψ itself not vanish at infinity, equation (A1) shows that we must have $a_0 \neq 0$. Then the flux function at infinity is given by

$$\psi(r = \infty) = a_0[P_{l-1}(\mu) - P_{l+1}(\mu)] = a_0(1 - \mu) .$$

This equation shows that the open field at infinity takes on the " split monopole " configuration regardless of the flux distribution at the coronal base. Because the value of ψ is constant on each field line, the range of ψ values at infinity must be the same as at the base, and this immediately requires that $a_0 = \psi_0$.

Now, in this open-field case there is a current sheet in the equatorial plane, and we require different solutions in the two hemispheres. Here we solve explicitly in the northern hemisphere only; the southern hemisphere solution is obtained with suitable sign changes. To make the current sheet, we require that $B_\theta = 0$ in the equatorial plane. This condition can be met if the Legendre polynomials in equation (A4) are all odd, requiring that the values of l be even. So we now have

$$\psi_{\mathrm{open}}(r, \mu) = \psi_0(1 - \mu) + \sum_{l=2,4,\ldots}^{\infty} a_l r^{-l} \left[\frac{P_{l-1}(\mu) - P_{l+1}(\mu)}{2l+1} \right] .$$

Again, orthogonality of the Legendre polynomials leads to a recursion relation,

$$a_{m+1} = (2m+3) \left[\frac{a_{m-1}}{2m-1} + (2m+1)\psi_0 I_{m0} \right] , \tag{A5}$$

where

$$I_{m0} = \int_0^1 (\mu - \mu^\alpha) P_m(\mu) \, d\mu .$$

Note that this expression differs slightly from the analogous quantity for the closed-field case.

This completes the prescription for constructing Legendre series solutions in both the closed- and open-field cases, using the recursion relations (A3) and (A5) and associated definitions. It is then straightforward to evaluate the magnetic energies for different values of the flux distribution parameter α using the virial surface integral of equation (1). Again, this was done analytically using MATHEMATICA.

REFERENCES

Aly, J. J. 1984, ApJ, 283, 349
———. 1991, ApJ, 375, L61
Antiochos, S. K., Devore, C. R., & Klimchuk, J. A. 1999, ApJ, 510, 485
Bank, R. E. 1998, PLTMG: A Software Package for Solving Elliptic Partial Differential Equations Users' Guide 8.0 (Philadelphia: Society for Industrial and Applied Mathematics)
Forbes, T. G., & Isenberg, P. A. 1991, ApJ, 373, 294
Klimchuk, J. A. 2001, in Space Weather: Geophysical Monograph Ser. 125, ed. P. Song, H. Singer, & G. Siscoe (Washington, American Geophysical Union), 143
Klimchuk, J. A., & Sturrock, P. A. 1989, ApJ, 345, 1034
Low, B. C. 1977, ApJ, 212, 234
Lynden-Bell, D., & Boily, C. 1994, MNRAS, 267, 146
Priest, E. R. 1984, Solar Magneto-Hydrodynamics (Dordrecht: Reidel), 108
Sturrock, P. A. 1991, ApJ, 380, 655
Wolfson, R. 1985, ApJ, 288, 769
———. 1995, ApJ, 443, 810
Wolfson, R., & Low, B. C. 1992, ApJ, 391, 353
Yang, W. H., Sturrock, P. A., & Antiochos, S. K. 1986, ApJ, 309, 383